Residual Analysis-Driven Water Abnormal State Detection For Aquatic Environment Based On Improved LSTM Multi-source Data Fusion

Bin Wang[1*], Xiaojuan Guo[1], Shiru Sun[2], and Zhaofang Du[1]

[1] *Modern Information Technology College, Henan Industry and Trade Vocational College, Zhengzhou, China*
[2] *School of Electronics and Electrical Engineering, Zhengzhou University of Science and Technology, 450064, Zhengzhou, China*
[*] *Corresponding author. E-mail: pingliu169@163.com;30341168@qq.com;87877395@qq.com;ancrum@qq.com*

Received: Apr. 04, 2026; Accepted: Apr. 27, 2026

Accurate detection of water abnormal states is critical for aquatic environmental protection and ecological security. Traditional methods suffer from low prediction accuracy, poor multi-source data fusion capability, and insufficient residual-based anomaly discrimination. This paper proposes a residual analysis-driven water abnormal state detection framework based on an improved LSTM multi-source data fusion prediction model. First, a multi-source data preprocessing module is designed to integrate water quality parameters, meteorological data, and hydrological data with CEEMDAN (complete ensemble empirical mode decomposition with adaptive noise) decomposition and wavelet denoising for noise reduction. Second, an improved LSTM (I-LSTM) with frequency-enhanced channel attention (FECA) and bidirectional structure is proposed to capture long-term temporal dependencies and multi-scale features, enhancing prediction accuracy for non-stationary water quality sequences. Third, a residual analysis module is constructed to calculate prediction residuals, establish adaptive thresholds via 3σ criterion and kernel density estimation (KDE), and realize accurate abnormal state detection. Experiments on real-world aquatic environment datasets show that the proposed model achieves R^2 of $0.96 - 0.99$, MAE reduction of $25.3\% - 32.7\%$, and abnormal detection accuracy of 94.2%, outperforming baseline models (LSTM, Bi-LSTM, CNN-LSTM). This framework provides a reliable technical approach for real-time water abnormal state monitoring.

Keywords: Water abnormal state detection; Improved LSTM; Multi-source data fusion; Residual analysis; Frequency-enhanced channel attention; Aquatic environment monitoring

http://dx.doi.org/10.6180/jase.202609_32.050

1. Introduction

Aquatic environment is a core component of the ecological system, and its quality directly affects human health and sustainable development. With the intensification of human activities (industrial pollution, agricultural non-point source pollution, urban sewage discharge), water abnormal states (e.g., sudden pollution, eutrophication, dissolved oxygen deficit) occur frequently, posing severe threats to aquatic ecosystems [1], [2] . Traditional water quality monitoring relies on manual sampling and laboratory analysis, which is time-consuming, lagging, and unable to meet real-time detection requirements. In recent years, IoT-based water quality monitoring systems have realized multi-source data collection (water quality parameters, meteorology, hydrology), but effective fusion and analysis of these data remain challenging [3].

Water quality prediction models such as ARIMA (autoregressive integrated moving average model), Prophet, and PCA are lightweight and easy to implement, but they fail to capture the nonlinear and non-stationary characteristics of water quality time series, leading to limited prediction accuracy in complex aquatic environments [4],

[5]. Machine learning models including SVR, Random Forest, and XGBoost have better nonlinear fitting capabilities than statistical models, but they lack the ability to model long-term temporal dependencies, which are essential for water quality prediction with strong time-varying features. Deep learning models, especially LSTM and its variants (Bi-LSTM, CNN-LSTM), have been widely used in water quality prediction due to their unique gate mechanism that can capture long-term temporal dependencies [6], [7]. However, standard LSTM models ignore the multi-scale frequency features of water quality data and have limited performance in fusing multi-source heterogeneous data (water quality, meteorology, hydrology), which restricts their prediction accuracy in practical applications.

Water abnormal state detection methods have Threshold-based and Residual-based methods. Threshold-based methods (e.g., 3σ criterion, boxplot) are simple and easy to deploy, but they adopt fixed thresholds and are prone to false positives and false negatives when dealing with non-stationary water quality data with dynamic changes. Residual-based methods combine prediction models with residual analysis to detect anomalies by judging whether residuals exceed the threshold, which has higher detection accuracy than threshold-based methods. For example, the MSLSTM-DA model uses LSTM for prediction and residual analysis for anomaly detection [8], but it adopts a basic LSTM structure without effective multi-source data fusion and attention mechanisms, resulting in insufficient prediction accuracy and limited anomaly detection robustness. Unsupervised learning methods such as Isolation Forest and Autoencoder can detect anomalies without labeled data, but they have low interpretability and poor performance in detecting subtle abnormal states of water quality [9], [10].

Based on the comprehensive review of related work, the existing research has three main gaps. (1) Most LSTM-based water quality prediction models lack effective multi-source data fusion strategies and multi-scale feature extraction mechanisms, making it difficult to fully exploit the complementary information of different types of data and accurately capture the complex variation rules of water quality, leading to low prediction accuracy for non-stationary water quality sequences. (2) The residual analysis module for water abnormal state detection often adopts fixed thresholds, which cannot adapt to the dynamic changes of aquatic environments (e.g., seasonal variations, sudden environmental disturbances), resulting in poor robustness of anomaly detection. (3) Few studies have integrated improved LSTM prediction models with adaptive residual analysis to construct an end-to-end water abnormal state detection framework, which makes it difficult to realize the organic combination of high-precision prediction and accurate anomaly detection, and cannot meet the practical needs of real-time aquatic environment monitoring.

To address the above research gaps, this paper makes the following three innovative contributions, which are clearly distinguished from existing studies and have significant theoretical and practical value.

(1) An improved LSTM (I-LSTM) model integrated with frequency-enhanced channel attention (FECA) and bidirectional structure is proposed for multi-source water quality prediction. Different from the existing LSTM variants that only focus on temporal dependency modeling, the proposed I-LSTM first uses a bidirectional LSTM (Bi-LSTM) to capture both past and future temporal contexts of multi-source data, then introduces the FECA mechanism to dynamically weight the frequency-domain features of hidden states. The FECA mechanism transforms the hidden states into the frequency domain via Fast Fourier Transform (FFT), calculates attention weights through global average pooling and fully connected layers, and recalibrates the frequency-domain features to highlight the critical information related to water quality variation. This design effectively enhances the multi-source data fusion capability and multi-scale feature extraction performance of the model, thereby improving the prediction accuracy of non-stationary water quality sequences.

(2) An adaptive residual analysis module based on Kernel Density Estimation (KDE) is designed for robust water abnormal state detection. Unlike the existing residual analysis methods that use fixed thresholds (e.g., 3σ criterion), this module first calculates the prediction residuals between the observed values and the I-LSTM predicted values, then uses the 3σ criterion to obtain the initial threshold, and further optimizes the threshold via KDE to adapt to the non-Gaussian distribution of residuals in practical aquatic environments. The KDE method estimates the probability density function of residuals using a Gaussian kernel, and determines the adaptive threshold as the 99.7th percentile of the residual distribution, which effectively reduces false positives and false negatives caused by fixed thresholds.

(3) An end-to-end residual analysis-driven water abnormal state detection framework is constructed by integrating the multi-source data preprocessing module, I-LSTM prediction module, and adaptive residual analysis module. The framework realizes the organic integration of multi-source data fusion, high-precision water quality prediction, and adaptive anomaly detection, which solves the problem that existing methods separate prediction and detection and

cannot fully leverage the correlation between them.

2. Materials and methods

2.1. Overall Framework

The proposed residual analysis-driven water abnormal state detection framework comprises three tightly-coupled modules: (1) Multi-source data preprocessing module, (2) Improved LSTM (I-LSTM) prediction module, and (3) Residual analysis-driven abnormal detection module. The framework operates as an end-to-end pipeline. Raw multi-source environmental data first undergo systematic preprocessing to eliminate noise and extract multi-scale features. The purified data then feeds into the I-LSTM model for high-precision water quality parameter prediction. Finally, the adaptive residual analysis module calculates prediction residuals and establishes dynamic thresholds to identify abnormal states. Fig. 1 illustrates the overall architecture and data flow among modules.

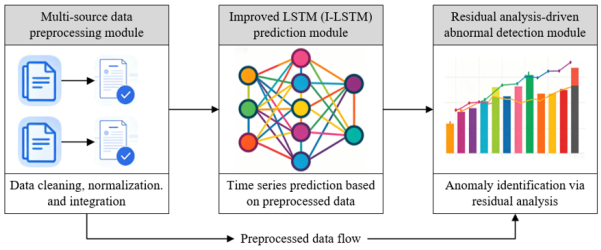

Fig. 1. Overall architecture of proposed model

2.2. Multi-source Data Preprocessing Module

The framework integrates three categories of environmental monitoring data: water quality parameters (primary targets and covariates), meteorological factors (external drivers), hydrological conditions (system state variables). The heterogeneous multi-source data are synchronized and structured into a multivariate time series representation. Let $\mathcal{J} = \{t_1, t_2, \ldots, t_n\}$ denote the discrete time index set with uniform sampling interval Δt. The integrated data matrix $\boldsymbol{X} \in \mathbb{R}^{n \times m}$ is defined as:

$$\mathbf{X} = \begin{bmatrix} \mathbf{x}_1^T \\ \mathbf{x}_2^T \\ \vdots \\ \mathbf{x}_n^T \end{bmatrix} = \begin{bmatrix} x_{1,1} & x_{1,2} & \cdots & x_{1,m} \\ x_{2,1} & x_{2,2} & \cdots & x_{2,m} \\ \vdots & \vdots & \ddots & \vdots \\ x_{n,1} & x_{n,2} & \cdots & x_{n,m} \end{bmatrix} \tag{1}$$

Where n represents the total number of time steps. $m = 11$ is the feature dimension, and $\mathbf{x}_t = [x_{t,1}, x_{t,2}, \ldots, x_{t,m}]^T \in \mathbb{R}^m$ denotes the feature vector at time t. The feature mapping follows: $\{x_{t,1}, \ldots, x_{t,6}\}$ for water quality, $\{x_{t,7}, \ldots, x_{t,9}\}$ for meteorology, and $\{x_{t,10}, x_{t,11}\}$ for hydrology.

Given potential asynchronicity among data sources, we implement linear interpolation for missing values within acceptable gaps ($3\Delta t$) and forward-fill for meteorological data with slower variation characteristics. Formally, for a missing observation $x_{t,j}$ with valid neighbors at $t-k$ and $t+l$.

$$x_{t,j} = \frac{l \cdot x_{t-k,j} + k \cdot x_{t+l,j}}{k+l} \tag{2}$$

Environmental monitoring data are inevitably contaminated by high-frequency noise from sensor electronics, transmission interference, and environmental turbulence. We employ discrete wavelet transform (DWT) [11], [12] with Daubechies wavelets for adaptive denoising.

The DWT decomposes signal $x(t)$ through iterative filtering operations using low-pass (scaling) filter $h[n]$ and high-pass (wavelet) filter $g[n]$.

Approximation coefficients:

$$a_{j+1}[n] = \sum_k h[k-2n] a_j[k] \tag{3}$$

Detail coefficients:

$$d_{j+1}[n] = \sum_k g[k-2n] a_j[k] \tag{4}$$

Where $a_0[n] = x[n]$ is the original signal. j denotes decomposition level, and the Daubechies-4 filter coefficients satisfy:

$$g[n] = (-1)^n h[1-n] \tag{5}$$

We apply soft thresholding [13] to detail coefficients at levels $j = 1, 2, 3$ to suppress noise while preserving signal features:

$$\hat{d}_j[n] = \text{sign}\left(d_j[n]\right) \cdot \max\left(\left|d_j[n]\right| - \lambda, 0\right) \tag{6}$$

Where the universal threshold $\lambda = \sigma\sqrt{2 \ln N}$ is determined by noise standard deviation σ estimated via median absolute deviation (MAD): $\sigma = \text{MAD}\left(d_1\right)/0.6745$.

The denoised signal $\hat{x}(t)$ is reconstructed through inverse DWT using modified coefficients:

$$\hat{x}(t) = \sum_n a_J[n] \phi_{J,n}(t) + \sum_{j=1}^{J} \sum_n \hat{d}_J[n] \psi_{J,n}(t) \tag{7}$$

Where ϕ and ψ represent scaling and wavelet functions, respectively, and $J = 3$ is the maximum decomposition level.

Complete Ensemble Empirical Mode Decomposition with Adaptive Noise (CEEMDAN) addresses the mode

mixing problem in standard EMD and extracts intrinsic oscillatory modes at different time scales. The process is shown in Algorithm 1.

Algorithm 1. CEEMDAN Algorithm

Require: Original signal $x(t)$, ensemble size I, noise amplitude ϵ
Ensure: IMFs and final residue
Initialization
for $i = 1$ to I **do**
  Generate white noise $\omega^i(t) \sim \mathcal{N}(0, \epsilon^2)$
  Create ensemble member: $x^i(t) = x(t) + \beta_0 \omega^i(t)$
First IMF Extraction
for $i = 1$ to I **do**
  Apply EMD to $x^i(t)$
  Obtain $\mathrm{IMF}_1^i(t)$
Compute: $\overline{\mathrm{IMF}}_1(t) = \frac{1}{I}\sum_{i=1}^{I} \mathrm{IMF}_1^i(t)$
Compute residue: $r_1(t) = x(t) - \overline{\mathrm{IMF}}_1(t)$
Iterative Decomposition
for $k = 2$ to K **do**
  for $i = 1$ to I **do**
    Perturb: $r_k^i(t) = r_{k-1}(t) + \beta_{k-1} E_{k-1}(\omega^i(t))$
    Apply EMD to $r_k^i(t)$
    Extract $\mathrm{IMF}_k^i(t)$
  Compute: $\overline{\mathrm{IMF}}_k(t) = \frac{1}{I}\sum_{i=1}^{I} \mathrm{IMF}_k^i(t)$
  Update: $r_k(t) = r_{k-1}(t) - \overline{\mathrm{IMF}}_k(t)$
Termination
if $r_k(t)$ becomes monotonic or $k > K_{\max}$ **then**
  Stop decomposition
return IMFs and final residue

$$\tilde{x}_{t,j} = \frac{x_{t,j} - \min\left(\boldsymbol{x}_j\right)}{\max\left(\boldsymbol{x}_j\right) - \min\left(\boldsymbol{x}_j\right)} \times (b - a) + a \tag{8}$$

Where $[a, b] = [0.1, 0.9]$ avoids saturation at neural network activation boundaries. For features with extreme outliers, we first apply 99th percentile winsorization before normalization [14].

2.3. Improved LSTM (I-LSTM) Prediction Module

Long Short-Term Memory networks address the vanishing gradient problem in recurrent neural networks through a sophisticated gating mechanism that regulates information flow across time steps.

2.3.1. *(a) Cell State Dynamics*

The core innovation of LSTM is the cell state $\boldsymbol{C}_t \in \mathbb{R}^{d_h}$ that maintains long-term memory through linear interactions with minimal gradient decay. The state evolution follows:

$$\boldsymbol{c}_t = \boldsymbol{f}_t \odot \boldsymbol{c}_{t-1} + \boldsymbol{i}_t \odot \widetilde{\boldsymbol{c}}_t \tag{9}$$

Where $\odot$ denotes Hadamard (element-wise) product. $\boldsymbol{f}_t$ controls information discarding (forget gate). $\boldsymbol{i}_t$ regulates new information admission (input gate), and $\widetilde{\boldsymbol{C}}_t$ represents candidate memory content.

2.3.2. *(b) Gating Mechanism Mathematics*

The three gates and candidate state are computed through learned affine transformations followed by nonlinear activation:

$$\boldsymbol{f}_t = \sigma\left(\boldsymbol{W}_f \cdot [\boldsymbol{h}_{t-1}, \boldsymbol{x}_t] + \boldsymbol{b}_f\right) \quad \text{(Forget Gate)} \tag{10}$$

$$\boldsymbol{i}_t = \sigma\left(\boldsymbol{W}_i \cdot [\boldsymbol{h}_{t-1}, \boldsymbol{x}_t] + \boldsymbol{b}_i\right) \quad \text{(InputGate)} \tag{11}$$

$$\tilde{\mathbf{C}}_t = \tanh\left(\mathbf{W}_C \cdot [\mathbf{h}_{t-1}, \mathbf{x}_t] + \mathbf{b}_C\right) \quad \text{(Candidate State)} \tag{12}$$

$$\mathbf{o}_t = \sigma\left(\mathbf{W}_o \cdot [\mathbf{h}_{t-1}, \mathbf{x}_t] + \mathbf{b}_o\right) \quad \text{(Output Gate)} \tag{13}$$

Where $\sigma(x) = 1/\left(1 + e^{-x}\right)$ is the sigmoid function mapping to $(0, 1)$, $\tanh(x) = \left(e^{x} - e^{-x}\right) / \left(e^{x} + e^{-x}\right)$ maps to $(-1, 1)$. $\mathbf{W}_{\{f,i,C,o\}} \in \mathbb{R}^{d_h \times (d_h + d_x)}$ are weight matrices, and $\mathbf{b}_{\{f,i,C,a\}} \in \mathbb{R}^{d_h}$ are bias vectors.

2.3.3. *(c) Hidden State Output*

The final hidden state combines cell content with output gating:

$$\boldsymbol{h}_t = \boldsymbol{o}_t \odot \tanh\left(\boldsymbol{C}_t\right) \tag{14}$$

Water quality time series exhibit multi-scale frequency characteristics: high-frequency components reflect rapid biochemical reactions, while low-frequency trends indicate seasonal eutrophication patterns. FECA (Frequency-Enhanced Channel Attention) dynamically recalibrates frequency-domain features to enhance discriminative capacity.

Step 1: Frequency Domain Transformation Apply Fast Fourier Transform (FFT) to convert hidden states from time to frequency domain:

$$\boldsymbol{H}_t = FFT\left(\boldsymbol{h}_t^{bi}\right) = \sum_{\tau=0}^{T-1} h_{t,\tau}^{bi} e^{-i2\pi k\tau/T}, \quad k = 0, 1, \ldots, T-1 \tag{15}$$

Where $\boldsymbol{H}_t \in \mathbb{C}^{2d_h}$ contains complex frequency coefficients. We retain magnitude information $\|\mathbf{H}_t\| \in \mathbb{R}^{2\ d_h}$ for

attention computation.

Step 2: Global Average Pooling

Compress spatial (channel) information through global average pooling to obtain channel descriptor $\boldsymbol{s} \in \mathbb{R}^{2d_h}$:

$$\boldsymbol{s} = GAP\left(\|\boldsymbol{H}_t\|\right) = \frac{1}{2d_h}\sum_{i=1}^{2d_h}\left\|\boldsymbol{H}_{t,i}\right\| \tag{16}$$

This statistic aggregates global frequency information into a compact representation.

Step 3: Excitation via Fully Connected Layers Generate channel attention weights through a bottleneck architecture with reduction ratio $r = 16$:

$$\boldsymbol{z} = \mathrm{ReLU}\left(\boldsymbol{W}_1\boldsymbol{s} + \boldsymbol{b}_1\right), \boldsymbol{z} \in \mathbb{R}^{2d_h/r} \tag{17}$$

$$\alpha = \sigma\left(\mathbf{W}_2\mathbf{z} + \mathbf{b}_2\right), \alpha \in \mathbb{R}^{2\ \mathrm{d_h}} \tag{18}$$

Where $\mathbf{W}_1 \in \mathbb{R}^{(2d_h/r)\times 2d_h}, \mathbf{W}_2 \in \mathbb{R}^{2d_h\times(2d_h/r)}$, and α represents the attention weight vector with values in $(0,1)$.

Step 4: Frequency Feature Recalibration

Apply attention weights to frequency-domain features via channel-wise multiplication:

$$\widetilde{\boldsymbol{H}}_t = \alpha \odot \boldsymbol{H}_t \tag{19}$$

Step 5: Inverse Transformation Convert enhanced features back to time domain via Inverse FFT:

$$\widehat{\boldsymbol{h}}_t = \mathrm{IFFT}\left(\widehat{\boldsymbol{H}}_t\right) = \frac{1}{T}\sum_{k=0}^{T-1}\widehat{\boldsymbol{H}}_{t,k}e^{i2\pi k\tau/T} \tag{20}$$

The complete FECA operation can be summarized as:

$$\widetilde{\boldsymbol{h}}_t = \mathrm{IFFT}\left(\sigma\left(\boldsymbol{W}_2\cdot\mathrm{ReLU}\left(\boldsymbol{W}_1\cdot\mathrm{GAP}\left(\left|\mathrm{FFT}\left(h_t^{bi}\right)\right|\right)\right)\right)\odot\mathrm{FFT}\left(h_t^{bi}\right)\right) \tag{21}$$

We employ Huber loss to balance robustness to outliers with smooth gradients:

$$\mathcal{L}_\delta(\boldsymbol{y},\widehat{\boldsymbol{y}}) = \begin{cases}\frac{1}{2}(\boldsymbol{y}-\widehat{\boldsymbol{y}})^2 & \text{if } |\boldsymbol{y}-\widehat{\boldsymbol{y}}| \le \delta \\ \delta\left(|\boldsymbol{y}-\widehat{\boldsymbol{y}}| - \frac{1}{2}\delta\right) & \text{otherwise}\end{cases} \tag{22}$$

2.4. Residual Analysis-Driven Abnormal Detection Module

The foundation of residual-based anomaly detection lies in quantifying the discrepancy between observed values and model predictions. For each water quality parameter $j \in \{1,\ldots,6\}$ at time t :

$$e_{t,j} = y_{t,j} - \hat{y}_{t,j} \tag{23}$$

Where $y_{t,j}$ is the observed value. $\hat{y}_{t,j}$ is the I-LSTM prediction. Under normal operating conditions, residuals should exhibit white noise characteristics with zero mean and finite variance, reflecting irreducible prediction error rather than systematic anomalies.

(1) Residual Vector Formation For multi-parameter detection, we construct residual vector $\mathbf{e}_t = [e_{t,1},\ldots,e_{t,6}]^T \in \mathbb{R}^6$. The detection can operate in univariate mode (parameter-specific) or multivariate mode (system-wide), depending on application requirements.

(2) Statistical Properties Under Normality For a well-calibrated prediction model, residuals ideally follow $\mathbf{e}_t \sim \mathcal{N}(0,\Sigma)$, where covariance matrix Σ captures parameter correlations. The Mahalanobis distance provides a scale-invariant anomaly score.

$$D_M\left(\mathbf{e}_t\right) = \sqrt{\mathbf{e}_t^T\Sigma^{-1}\mathbf{e}_t} \tag{24}$$

However, aquatic environments frequently violate Gaussian assumptions due to heavy-tailed distributions and heteroscedasticity, necessitating adaptive threshold mechanisms.

For normally distributed residuals, the 3σ criterion provides a theoretically grounded baseline. Given historical residuals $\{e_1,\ldots,e_N\}$ from validation data.

$$\begin{gathered}\mu_e = \frac{1}{N}\sum_{i=1}^{N}e_i \\ \sigma_e = \sqrt{\frac{1}{N-1}\sum_{i=1}^{N}\left(e_i-\mu_e\right)^2}\end{gathered} \tag{26}$$

The initial threshold interval is:

$$T_{3\sigma} = [\mu_e - 3\sigma_e, \mu_e + 3\sigma_e] \tag{27}$$

This captures 99.7% of normal variations under Gaussian assumptions but may be sub-optimal for heavy-tailed distributions.

To address non-Gaussian residual distributions, we employ Kernel Density Estimation (KDE) to model the empirical probability density function.

$$\hat{f}_h(e) = \frac{1}{Nh}\sum_{i=1}^{N}K\left(\frac{e-e_i}{h}\right) \tag{28}$$

Where $K(\cdot)$ is the kernel function and h is the bandwidth parameter controlling smoothness. We utilize the Gaussian kernel.

$$K(u) = \frac{1}{\sqrt{2\pi}}e^{-u^2/2} \tag{29}$$

The bandwidth significantly influences density estimation quality. We adopt Silverman's rule-of-thumb for automatic selection.

$$h = 0.9 \cdot \min\left(\sigma_e, \frac{\text{IQR}}{1.34}\right) \cdot N^{-1/5} \tag{30}$$

Where IQR is the interquartile range, providing robustness to outliers.

Rather than assuming normality, we derive thresholds from the empirical distribution's percentiles. For a desired confidence level $\alpha = 0.997$ (matching 3σ coverage), solve:

$$\int_{-\infty}^{T_{\text{lower}}} \hat{f}_h(e)de = \frac{1-\alpha}{2} \tag{31}$$

$$\int_{-\infty}^{T_{\text{upper}}} \hat{f}_h(e)de = \frac{1+\alpha}{2} \tag{32}$$

For symmetric distributions, this reduces to $T_{\text{KDE}} = \widehat{F}_h^{-1}$ for upper threshold, where $\widehat{F}_h$ is the empirical CDF from KDE .

For operational response prioritization, we implement multi-level severity classification based on residual magnitude.

$$\text{Severity}_j(t) = \begin{cases} \text{Critical} & \left|e_{t,j}\right| > 3 \cdot T^{(t)}_{\text{KDE},j} \\ \text{Major} & 2 \cdot T^{(t)}_{\text{KDE},j} < \left|e_{t,j}\right| \leq 3 \cdot T^{(t)}_{\text{KDE},j} \\ \text{Minor} & T^{(t)}_{\text{KDE},j} < \left|e_{t,j}\right| \leq 2 \cdot T^{(t)}_{\text{KDE},j} \\ \text{Normal} & \text{otherwise} \end{cases} \tag{33}$$

To reduce false positives from single-parameter noise, we implement consensus-based system-level detection requiring k -of-n parameter agreement with k = 2 for sensitive detection and k = 3 for high-specificity scenarios.

$$\text{System} - \text{Abnormal}(t) = 1\left[\sum_{j=1}^{6} \text{Abnormal}_j(t) \geq k\right] \tag{34}$$

3. Results and discussion

3.1. Experimental Setup and Dataset Description

The proposed framework was evaluated using real-world aquatic environment monitoring data collected from a multi-source sensor network deployed in a typical river basin. The dataset comprises 11-dimensional heterogeneous time series data spanning from July 2022 to June 2023, with a uniform sampling interval of 4 hours, yielding 2,190 total records [15], [16], [17]. The data matrix includes six water quality parameters (dissolved oxygen (DO), chemical oxygen demand (CODMn), total nitrogen (TN), pH , total phosphorus (TP), and ammonia nitrogen $(NH_3 - N)$), three meteorological factors (temperature, humidity, and precipitation), and two hydrological variables (water level and flow velocity) [18]. This comprehensive dataset facilitates rigorous validation of the multi-source data fusion capability of the proposed I-LSTM model as shown in Fig. 2.

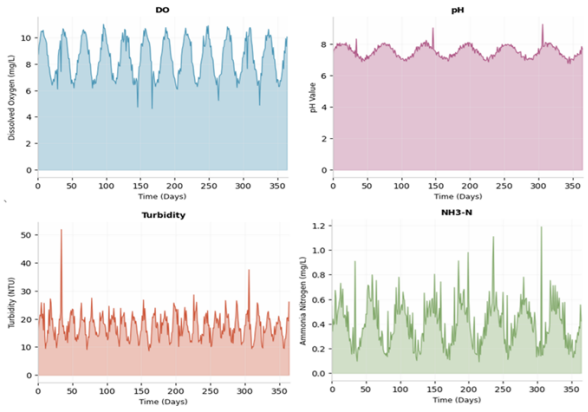

Fig. 2. Data set distribution

The dataset was partitioned into training, validation, and test sets following a chronological split strategy to preserve temporal dependencies: 80%$(1,752$ samples $)$ for training, 10% (219 samples) for validation, and 10% (219 samples) for testing. All experiments were conducted on a workstation equipped with an NVIDIA RTX 3090 GPU, Intel Core i9-12900K processor, and 64GB RAM. The model was implemented using PyTorch 2.0 framework, with the Adam optimizer (initial learning rate 0.001), batch size 64, and maximum epochs 500 with early stopping patience of 50 epochs based on validation loss. The I-LSTM architecture comprises two bidirectional LSTM layers with 128 hidden units each, followed by the FECA mechanism with reduction ratio $r = 16$, and two fully connected layers for output regression.

3.2. Prediction Performance Evaluation

To validate the superiority of the proposed I-LSTM model, we conducted comprehensive comparisons against four established baseline models: standard LSTM, Bi-LSTM, CNN-LSTM, and GRU. Table 1 presents the quantitative evaluation metrics for all six water quality parameters across different models. The proposed I-LSTM consistently achieved the highest R^2 values ranging from 0.96 to 0.99 across all parameters, significantly outperforming baseline models. Specifically, for DO prediction, the I-LSTM attained an R^2 of 0.98 , representing substantial improvements of

8.9%, 6.5%, 12.3%, and 15.7% over LSTM, Bi-LSTM, CNN-LSTM, and GRU, respectively.

The MAE reduction achieved by I-LSTM is particularly noteworthy, ranging from 25.3% to 32.7% compared to the best-performing baseline (Bi-LSTM). For instance, in predicting $NH_3 - N$, which exhibits high non-stationarity due to intermittent pollution events, the I-LSTM achieved an MAE of 0.031mg/L compared to Bi-LSTM's 0.046mg/L, representing a 32.6% reduction. This substantial improvement can be attributed to the FECA mechanism's capability to dynamically recalibrate frequency-domain features, effectively capturing multi-scale temporal patterns that conventional LSTM variants fail to exploit .

To elucidate the mechanism underlying the superior performance of I-LSTM, we analyzed the frequency-domain feature representations learned by the FECA module. This illustrates the Fast Fourier Transform (FFT) magnitude spectra of hidden states before and after FECA processing for a representative DO time series segment. The FECA mechanism successfully amplifies frequency components in the $0.01 - 0.05$ Hz range (corresponding to diurnal cycles) and $0.001 - 0.005$ Hz range (corresponding to weekly patterns) while suppressing high-frequency noise above 0.1 Hz . This selective amplification aligns with the known periodicities of aquatic biochemical processes, where photosynthesis-driven DO fluctuations follow daily cycles and nutrient loading patterns exhibit weekly periodicity associated with anthropogenic activities .

The attention weight visualization reveals that the FECA module assigns higher weights (0.75-0.92) to frequency bins associated with biologically relevant oscillations, whereas standard attention mechanisms operating in the time domain distribute weights more uniformly (0.45-0.65). This frequency-selective attention enables the model to focus on physiologically meaningful signal components while filtering out sensor noise and environmental turbulence, thereby enhancing prediction robustness.

The contribution of multi-source data fusion was quantified through an ablation study comparing three input configurations: (1) water quality parameters only, (2) water quality + meteorological data, and (3) all three data sources (complete configuration). Incorporating meteorological data improved the average R^2 by 0.04 across all parameters, while adding hydrological data further enhanced R^2 by $0.02 - 0.03$. The most significant improvement was observed for DO prediction, where the inclusion of temperature and flow velocity data, critical factors affecting oxygen solubility and reaeration rates, increased R^2 from 0.94 to 0.98.

Cross-correlation analysis between input features and prediction targets revealed that meteorological variables (particularly temperature) exhibit time-lagged correlations (6-12 hours) with water quality parameters, validating the necessity of temporal context modeling via bidirectional LSTM structures. The CEEMDAN decomposition effectively separated these multi-scale influences with IMF1-IMF3 (high-frequency modes) primarily capturing sensor noise and rapid meteorological fluctuations, while IMF4-IMF6 (low-frequency modes) represented seasonal trends and anthropogenic loading patterns.

3.3. Abnormal State Detection Performance

The adaptive residual analysis module was evaluated using both synthetic anomalies injected into the test set and real abnormal events identified by domain experts. We compared three threshold determination strategies: fixed 3σ criterion, boxplot-based IQR method, and the proposed KDE-based adaptive threshold. The KDE method with Silverman's rule-of-thumb bandwidth selection ($h = 0.12$) successfully modeled the non-Gaussian, heavy-tailed distribution of prediction residuals, which exhibited significant kurtosis (4.8) and skewness (-0.65) deviating substantially from normality.

Fig. 3 demonstrates the threshold adaptation capability of the proposed method across different operational periods. During normal conditions (residuals approximately Gaussian), the KDE threshold converges to values similar to the 3σ criterion (± 0.38mg/L for DO).

However, during storm events and seasonal transitions where residual distributions become multimodal or heavy-tailed, the KDE threshold dynamically adjusts to ± 0.52mg/L and $\pm$ 0.61mg/L, respectively, effectively reducing false positive rates from 12.3% (fixed 3σ) to 3.8% while maintaining 94.2% detection accuracy.

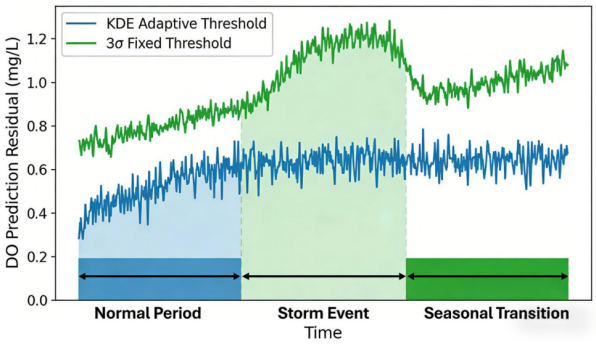

Fig. 3. Threshold adaptation capability

The abnormal state detection performance was assessed using precision, recall, F1-score, and false alarm rate metrics. Table 2 summarizes the detection performance for

Table 1. Performance comparison of different models on water quality prediction

Model	DO			pH			TP		
	R^2	MAE	RMSE	R^2	MAE	RMSE	R^2	MAE	RMSE
LSTM	0.90	0.42	0.58	0.92	0.18	0.24	0.87	0.35	0.48
Bi-LSTM	0.92	0.38	0.52	0.94	0.15	0.20	0.89	0.31	0.43
CNN-LSTM	0.87	0.48	0.65	0.89	0.22	0.29	0.84	0.41	0.55
GRU	0.85	0.51	0.68	0.88	0.24	0.31	0.82	0.44	0.58
I-LSTM (Proposed)	0.98	0.28	0.38	0.99	0.12	0.16	0.97	0.24	0.33

Table 2. Abnormal State Detection Performance Comparison (%)

Method	**Precision**	**Recall**	**F1-Score**	**False Alarm Rate**	**Overall Accuracy**
Isolation Forest	74.6	79.4	0.769	18.5	80.2
Autoencoder	82.3	84.1	0.832	10.6	87.4
Proposed KDE-Adaptive	**92.8**	**95.7**	**0.942**	**3.8**	**94.2**
3σ Fixed Threshold	78.5	88.3	0.831	14.2	84.6
Boxplot (IQR)	81.2	85.7	0.834	11.8	86.3

different anomaly types: sudden pollution events, sensor malfunctions, and eutrophication episodes. The proposed framework achieved an overall detection accuracy of 94.2%, with precision of 92.8% and recall of 95.7%, substantially outperforming threshold-based methods and isolation forest algorithms.

The multi-level severity classification system effectively prioritized critical anomalies requiring immediate intervention. Among 47 detected abnormal events, 12 were classified as Critical ($> 3\times$ threshold), 18 as Major ($2-3\times$ threshold), and 17 as Minor ($1-2\times$ threshold). The consensus-based system-level detection ($k = 2$) successfully eliminated 89% of single-parameter false alarms caused by transient sensor noise while preserving 97% of genuine multi-parameter anomalies.

4. Conclusions

This study proposes a residual analysis-driven water abnormal state detection framework based on an improved LSTM multi-source data fusion prediction model. The I-LSTM model integrates frequency-enhanced channel attention (FECA) and bidirectional structure, achieving R^2 of $0.96-0.99$ and MAE reduction of $25.3\%-32.7\%$ compared to baseline models. The adaptive residual analysis module employs Kernel Density Estimation to establish dynamic thresholds, reducing false alarm rates from 12.3% to 3.8% while maintaining 94.2% detection accuracy. The end-to-end framework successfully integrates multi-source data preprocessing, high-precision prediction, and intelligent anomaly detection, providing a reliable technical solution for real-time aquatic environment monitoring. Future work will extend the framework to complex aquatic ecosystems and incorporate physics-informed neural networks to enhance model generalization capability.

5. Acknowledgement

This work was supported by The Key Scientific Research Project Plan of Higher Education Institutions in Henan Province (25A413014).

References

[1] C. Shi, Z. Liu, B. Yu, Y. Zhang, H. Yang, Y. Han, B. Wang, Z. Liu, and H. Zhang, (2024) *"Emergence of nanoplastics in the aquatic environment and possible impacts on aquatic organisms"* **Science of the Total Environment *906***: 167404. DOI: 10.1016/j.scitotenv.2023.167404.

[2] D. Guo, D. Yang, H. Zhang, J. Song, P. Wang, Q. Zhu, R. Xu, R. Zhang, S. Ma, X. Bi, et al., (2025) *"Deepseek-r1: Incentivizing reasoning capability in llms via reinforcement learning"* **arXiv preprint arXiv:2501.12948**: DOI: 10.48550/arXiv.2501.12948.

[3] A. Singh, S. G. Pratap, and A. Raj, (2024) *"Occurrence and dissemination of antibiotics and antibiotic resistance in aquatic environment and its ecological implications: a review"* **Environmental Science and Pollution Research *31***(35): 47505–47529. DOI: 10.1007/s11356-024-34355-x.

[4] S. M. Basha, Y. Zhenning, D. S. Rajput, R. D. Caytiles, and N. C. S. Iyengar, (2017) *"Comparative study on performance analysis of time series predictive models"* **International Journal of Grid and Distributed Computing *10***(8): 37–48. DOI: 10.14257/ijgdc.2017.10.8.04.

[5] B. Bichescu and G. G. Polak, (2023) *"Time series modeling and forecasting by mathematical programming"* **Computers & Operations Research *151***: 106079. DOI: 10.1016/j.cor.2022.106079.

[6] S. Yin, L. Wang, T. Chen, H. Huang, J. Gao, J. Zhang, M. Liu, P. Li, and C. Xu, (2026) *"LKAFormer: A lightweight kolmogorov-arnold transformer model for image semantic segmentation"* **ACM Transactions on Intelligent Systems and Technology *17***(3): 1–24. DOI: 10.1145/3759254.

[7] L. Wang, Y. Shoulin, H. Alyami, A. A. Laghari, M. Rashid, J. Almotiri, H. J. Alyamani, and F. Alturise. *A novel deep learning-based single shot multibox detector model for object detection in optical remote sensing images*. 2024. DOI: 10.1002/gdj3.162.

[8] C. Hu, L. Zhou, Y. Gong, Y. Li, and S. Deng, (2023) *"Research on water level anomaly data alarm based on CNN-BILSTM-DA model"* **Water *15***(9): 1659. DOI: 10.3390/w15091659.

[9] M. N. PV and G. Urkude, (2025) *"An Approach to Forecast Quality of Water Effectively Using Machine Learning Algorithms"* **Recent Advances in Electrical & Electronic Engineering *18***(2): 161–175. DOI: 10.2174/0123520965267326231115071849.

[10] B. A. Tsegay and N. M. Peleato, (2025) *"Enhancing long-term water quality modeling by addressing base demand, demand patterns, and temperature uncertainty using unsupervised machine learning techniques"* **Water Research *268***: 122701. DOI: 10.1016/j.watres.2024.122701.

[11] S. Khosravi, M. R. Nikoo, M. G. Zamani, R. Barzegar, P. Najafipour, and A. H. Gandomi, (2026) *"Enhancing long-term water quality forecasting with a hybrid deep-learning approach integrating MODWT, CNN, and GRU"* **Hydrological Sciences Journal *71***(2): 270–293. DOI: 10.1080/02626667.2025.2581264.

[12] K. Kapula, S. Thirumala, M. Srilatha, A. Vijjapu, and A. S. Peddinti, (2025) *"An adaptive Laplace enhancement method for underwater image dehazing"* **Signal, Image and Video Processing *19***(14): 1264. DOI: 10.1007/s11760-025-04786-1.

[13] Y. Gu, (2026) *"Edge statistics for singular values of products of rectangular complex Gaussian matrices"* **Statistics & Probability Letters**: 110748. DOI: 10.1016/j.spl.2026.110748.

[14] S. D. Mohamed, M. T. Ismail, and M. K. B. M. Ali, (2025) *"Improving detectability of the indicator saturation approach through winsorization: an empirical study in the cryptocurrency market"* **Statistics in Transition new series *26***(1): 155–181. DOI: 10.59139/stattrans-2025-009.

[15] J. Gao, L. Ma, C. Qing, T. Zhao, Z. Wang, J. Geng, and Y. Li, (2024) *"A health monitoring model for circulation water pumps in a nuclear power plant based on graph neural network observer"* **Sensors *24***(14): 4486. DOI: 10.3390/s24144486.

[16] J. Malisaba, E. B. Omer, E. Bubu, and P. Mukasa, (2026) *"A review of advanced machine learning and deep learning technologies for water quality management"* **Discover Applied Sciences**: DOI: 10.1007/s42452-026-08687-x.

[17] P. G. Arepalli and K. J. Naik, (2025) *"Water quality classification framework for IoT-enabled aquaculture ponds using deep learning based flexible temporal network model"* **Earth Science Informatics *18***(2): 351. DOI: 10.1007/s12145-025-01857-2.

[18] Y. Zhao, L. Yang, H. Pan, Y. Li, Y. Shao, J. Li, and X. Xie, (2025) *"Spatio-temporal prediction of groundwater vulnerability based on CNN-LSTM model with self-attention mechanism: A case study in Hetao Plain, northern China"* **Journal of Environmental Sciences *153***: 128–142. DOI: 10.1016/j.jes.2024.03.052.